Desalination and Water Treatment
www.deswater.com
doi: 10.5004/dwt.2020.26239

204 (2020) 189–203
November

An efficient miniaturized flow cell loaded with magnetic nanoparticles for continuous removal of heavy metal ions

Hayat Abdulla Yusuf[a], Zainab Mohammed Redha[a,*], Sundus Zia[a], Zohair Sohail[a], K. Kombaiah[b], M. Bououdina[c], J. Judith Vijaya[b]

[a]*Department of Chemical Engineering, College of Engineering, University of Bahrain, P.O. Box: 32038, Bahrain, emails: zali@uob.edu.bh (Z. Mohammed Redha), hayousif@uob.edu.bh (H. Abdulla Yusuf), sundusnaik@hotmail.com (S. Zia), zohairsohail99@gmail.com (Z. Sohail)*
[b]*Catalysis and Nanomaterials Research Laboratory, Department of Chemistry, Loyola College (Autonomous), Chennai – 600 034, Tamil Nadu, India, emails: kombaiahloyola@gmail.com (K. Kombaiah), jjvijayaloyola@yahoo.com.in (J. Judith Vijaya)*
[c]*Department of Physics, College of Science, University of Bahrain, P.O. Box: 32038, Bahrain, email: mboudina@gmail.com (M. Bououdina)*

Received 27 January 2020; Accepted 10 June 2020

ABSTRACT

Magnetic ferrite nanoparticles were synthesized through the microwave-assisted combustion method. X-ray diffraction analysis confirmed the formation of a single spinel cubic structure with a mean crystallite size of 40–60 nm. Scanning electron microscopy observations revealed spherical-particles at the nanoscale with a tendency to agglomeration. Magnetic measurements indicated a ferromagnetic order with a saturation magnetization of 57–61 emu/g. A specially designed miniaturized flow cell was fabricated using a laser cutting machine on polymethyl methacrylate substrate. The flow cell was tailored to incorporate a magnet used to hold the nanoparticles in position while performing the flow experiments. The flow cell containing the nanoparticles was successfully applied for the removal of different heavy metal ions. Several factors affecting the adsorption of metal ions including pH, contact time, and flowrate, were investigated. Maximum adsorption efficiencies of 98%, 94% and 82% were achieved in almost 10 min for Cd(II), Cr(III) and Pb(II), respectively, while adsorption efficiencies of higher than 90% were obtained at around 40 min for Co(II) and Cu(II), and 50 min for Zn(II). The selectivity of nanoparticles for multiple metal ions solution varied in the order of Pb(II) > Cu(II) > Co(II) > Cd(II). Moreover, the synthesized nanoparticles proved their applicability for a real waste sample and their possibility to be regenerated with complete restoration of the adsorption efficiency. The adsorption of selective ions onto magnetic ferrite nanoparticles was found to follow pseudo-second-order kinetics and was well fitted by the Langmuir isotherm. This work provides an efficient method for the removal of heavy metal ions in continuous systems and complex environments, which make it a suitable candidate for industrial applications.

Keywords: Magnetic ferrite nanoparticles; Heavy metal ions; Flow cell; Continuous flow; Regeneration; Adsorption efficiency

1. Introduction

Because of the rapid development of industries and the expansion of the human population, more contaminants are brought up in wastewater, creating a huge threat to the aquatic ecosystem by deteriorating the quality of surface and groundwater. Many industries such as metal plating, pharmaceutical, textiles, semiconductors, food, fertilizer and pesticides, paper industries, etc., discharge billions of tons of wastewater containing many hazardous substances,

* Corresponding author.

namely heavy metals [1,2]. These metals, also known as trace metals, such as cobalt, zinc, copper, nickel, mercury, cadmium, lead and chromium, are one of the most persistent pollutants in wastewater. Thus, the discharge of heavy metal pollutants into water bodies present a serious threat to the environment and human health because of their toxicity and non-degradable characteristics, even at low concentrations [2,3]. This may also cause an upsurge in wastewater treatment costs.

To help mitigate the negative impacts of heavy metals toxicity in wastewater, there is an urgent need for adequate treatment of effluents before their discharge. For this, a variety of physicochemical and biological remediation processes exist. Technologies such as chemical precipitation [4,5], ion-exchange [6], adsorption [7,8], membrane filtration [9], coagulation-flocculation [1], and electrochemical methods [10] have been extensively studied in the literature and evaluated for the efficient removal of heavy metals from wastewater [2,3,11]. These methods have shown some drawbacks, including low removal efficiency, high-energy consumption, production of secondary and probably toxic waste, and high operating costs [12]. Naushad and AlOthman [13], investigated the removal of Pb(II) ions using acidic cation exchange resin, where they successfully achieved 88% removal efficiency. However, this efficiency was reduced to 74% after regenerations. In addition, such a method imposes other drawbacks, especially with large scales industrial applications, such as high operational costs, limited lifetime, removal of limited metals and the possibility of resins pollution in the presence of organic materials [3,14]. Heredia and Martín [15] reported 75% removal of Zn(II), Ni(II) and Cu(II) using a coagulation process with the aid of tannin-based flocculants. However, coagulation–flocculation suffers some limitations such as high operational costs, due to high chemical usage, as well as large volume and potential toxicity of the generated sludge [16]. Recently, permeable reactive barriers (PRBs) have been employed for the removal of lead ions from contaminated groundwater [17]. Excellent removal of 97% was achieved, yet there was neither report on possible regeneration of the bed, nor of any potential interference of other heavy metal ions on the disposal of the used sludge filter PRB.

Among the different treatment methods, nowadays, adsorption technology has emerged as an attractive method to overcome the aforementioned drawbacks. It is considered to be a facile, effective and economical method for heavy metals removal [3]. In adsorption processes, heavy metal ions are simply transferred from the contaminated water to the active sites on the surface of the adsorbent by physical or chemical means. Therefore, it produces high-quality treated effluents [3] without the generation of secondary waste [18]. It could be considered as a suitable and efficient alternative to the other methods owing to its wide adaptability, low operating and investment costs, simplicity of the design and operation as well as low fouling problems [3]. Additionally, the perused adsorbents can be regenerated by the desorption process and reused again with sufficient efficiency [12]. Consequently, the adsorption method has been gaining great interest in the field and has become one of the foremost techniques in wastewater treatment.

There are widespread categories of adsorption materials (adsorbents) for heavy metal ions removal, including mineral-based, organic-based or biological-based types [12]. For example, activated carbon is one of the well-known and widely investigated adsorbents for heavy metals removal, owing to its high surface area resulting in enhanced adsorption capacity. However, its large-scale industrial application is limited due to its relatively high-cost production and regeneration problems [19]. On the other hand, to meet the demand of large-scale industries, biosorbents could provide an alternative to activated carbon. These biomaterials have low cost and require minimum processing [20,21]. Along with cost and re-usability, the adsorption efficiency and uptake rapidity impose critical challenges on the process performance. Ideally, a good adsorbent should have sufficient available binding sites for heavy metal ions adsorption, thus, providing high capacities. These characteristics can be achieved at the nanoscale level [18]. Nanoparticles (NPs) offer profound advantages over conventional adsorbents due to their high surface-to-volume ratio, high dispersibility and shorter intraparticle diffusion distance [22]. Moreover, NPs are characterized by distinctive physical, chemical, and mechanical properties. These properties can be easily altered by a surface modification to improve the adsorption capacity and selectivity, thus increasing their potential for removing metal pollutants, even under complex environments [23]. Consequently, over the past few years, considerable research on the development of nano-adsorbent with unique characteristics has emerged [22]. Much research has revealed the significant role of magnetic nanocomposites in wastewater treatment. The combination of nanoscale adsorption and magnetic properties give such composites a unique capability of being easily separated from the treated water by the application of an external magnetic field [24]. These magnetic nanomaterials are also considered to be inexpensive, easily synthesized [25], and compatible with complex environments [24]. They can be synthesized from an element that has magnetic behavior such as iron, nickel, cobalt, in addition to zinc and magnesium; however, the former ion, particularly, iron oxide (Fe_3O_4), has attracted intensive attention for heavy metals removal [19,26,27].

In this paper, the synthesis and application of magnetic ferrite NPs for the removal of different heavy metal ions in a continuous system are investigated. For this study, cobalt-manganese ferrite ($CoMn)Fe_2O_4$ has been selected due to its inverse spinel structure in which metal ions occupy two sublattices [28]. It is also known to be inexpensive, has good chemical stability, efficient coupling, and high magnetostriction [28,29]. Moreover, this paper presents the fabrication of a novel, specially designed miniaturized flow cell using a laser cutting machine for the continuous adsorption of heavy metal ions. To the author's best knowledge, most adsorption studies were carried out in batch systems and no profound attention was given to continuous systems [22], yet all industrial treatment methods focus on flowing systems. Thus, this study examines the suitability of a low cost, efficient flow cell to overcome such drawbacks. The novel design, due to its continuous approach, reduces nanoparticle aggregation thus, enabling enhancement of adsorption capacity and stability. Furthermore, this paper investigates other important parameters for industrial large

scale applications such as the regeneration and reusability of the adsorbent. It also studies the influence of interfering metals and the selectivity of such nanoparticles toward specific heavy metal ions. The paper also discloses the compatibility of these nanoparticles with a real waste sample. Such studies seemed to be limited in the literature [22]. It has been reported that such magnetic nanoparticles have great potential for the treatment of some types of industrial waste as well as for many kinds of environmental remediation [30]. In recent work, such nanoparticles were successfully applied for the treatment of secondary effluent industrial wastewater [31]. Furthermore, in this paper, the effect of various operating conditions including pH, contact time, and solution flowrate on the adsorption efficiency was investigated. In addition, Freundlich and Langmuir's isotherms were examined to fit the adsorption model.

2. Experimental part

2.1. Materials

For NPs preparation, analytical grade cobalt nitrate ($Co(NO_3)_2{\cdot}6H_2O$), manganese nitrate ($Mn((NO_3)_2{\cdot}4H_2O$), ferric nitrate ($Fe(NO_3)_3{\cdot}9H_2O$) and urea $CO(NH_2)_2$ were purchased from Merck, India in their pure form. Cobalt nitrate, manganese nitrate, and ferric nitrate were taken as the precursors while urea was taken as the combustion agent.

For adsorption experiments, analytical grade cobalt nitrate ($Co(NO_3)_2{\cdot}6H_2O$), lead(II) nitrate $Pb(NO_3)_2$, cadmium nitrate ($Cd(NO_3)_2{\cdot}4H_2O$), zinc nitrate ($Zn(NO_3)_2{\cdot}6H_2O$), copper(II) nitrate ($Cu(NO_3)_2{\cdot}2.5H_2O$) and chromium nitrate ($Cr(NO_3){\cdot}3.9H_2O$) were all purchased from Research-Lab Fine Chem Industries, India. For pH adjustments, reagent grade hydrochloric acid (37 wt.%) was purchased from Scharlau (Spain) and sodium hydroxide (NaOH) was purchased from Timstar Laboratory Suppliers Ltd., (UK).

2.2. Characterization

X-ray diffraction (XRD) patterns were recorded using a high-resolution Rigaku Ultima IV diffractometer (Japan). Rietveld refinements were conducted using the PDXL program. Scanning electron microscopy (SEM) observations were taken using a VEGA 3 TESCAN equipped with a Bruker Nano (Germany) EDX detector for elemental chemical analysis. Magnetic measurements were performed at room temperature using a PMC MicroMag 3900 model vibrating sample magnetometer equipped a with 1T magnet. Magnetization curves were measured at room temperature from −10,000 to 10,000 Oe. Metal adsorption was measured using a WFX-110A/120A/130A atomic absorption spectrophotometer.

2.3. Synthesis of NPs

In the beginning, the components were dissolved in water and kept for dissolution by stirring for 30 min, using a magnetic stirrer, after which it was subjected to combustion in a microwave oven. The oven was set to 900 MHz at 540 W for 15 min. The burnt powders were cooled and thermally treated at 800°C for 2 h in a high-temperature furnace to improve chemical composition homogeneity and crystallinity.

2.4. Fabrication of the miniaturized flow cell

The flow cell was designed using the AUTODESK INVENTOR® software and fabricated at Awal Plastics Co., (Kingdom of Bahrain) using a laser cutting machine and computer numerical control software. Polymethyl methacrylate was selected as a substrate for the fabrication of the flow cell due to its specific properties, mainly, its permeability to the external magnetic field, which will be utilized to hold NPs in place, inside the flow cell. Other properties such as its surface stability, superior high-pressure resistance, as well as its availability at low cost were also considered.

The flow cell consisted of two parts: the base and the cover. The base part (Figs. 1a and c) consisted of the flow area (bed) where, the magnetic NPs were placed, and a compartment placed directly underneath the bed, for the insertion of a magnet. The cover part (Fig. 1b) had two circular holes on either end of the cell; each having a 1 mm diameter and 11.4 mm depth, representing the input and output of the flow. These holes were designed such that the wastewater would enter from the top of the cover and flow down to the base passing over the NPs bed.

Twelve equally spaced rectangular channels (1 mm height) coming out of the base part, at the *V*-shaped entrance and exit of the cell, were designed to evenly distribute the flow over the entire active area of the bed (flow chamber), as illustrated in Fig. 1a, thereby enhancing the contact between the fluid and magnetic NPs. Moreover, in order to fully seal the miniaturized flow cell, the cover was also designed to have channels coming out of it (0.5 mm height) but alternating to that of the base part (Fig. 1b), such that when the cell closes both parts are able to lock each other (Fig. 1c).

The dimensions for the miniaturized flow cell are shown in Fig. 2 and summarized in Table 1. The complete flow cell is shown in Fig. 3.

2.5. Adsorption experiments

A 1,000 mg/L stock solution of each heavy metal ion was prepared by dissolving 1 g of each heavy metal nitrate in distilled water. Samples of different concentrations were prepared from this stock solution by appropriate dilutions. A similar method was used to prepare the synthetic mixture solution, whereas the real waste sample was obtained from the Muharraq Wastewater Treatment Plant and was filtered to remove only solid impurities before treating it with NPs. This wastewater had a pH value of 7.7 and a conductivity of 3,669.4 μS/cm. The sample contained heavy metal ions such as Zn(II), Cd(II), Cu(II), Ni(II), Fe(III) for varying composition in the range 1.35 to 0.01 mg/L. The composition of Cu(II) was 0.12 mg/L while that of Cd(II) was 0.1 mg/L.

2.5.1. Batch experiments

For batch experiments, 4 mg/L of each solution was prepared by a dilution method to which 10 mg of equal ratio mixed NPs were added and the contents were mixed mechanically at 500 rpm with the help of an electric mixer

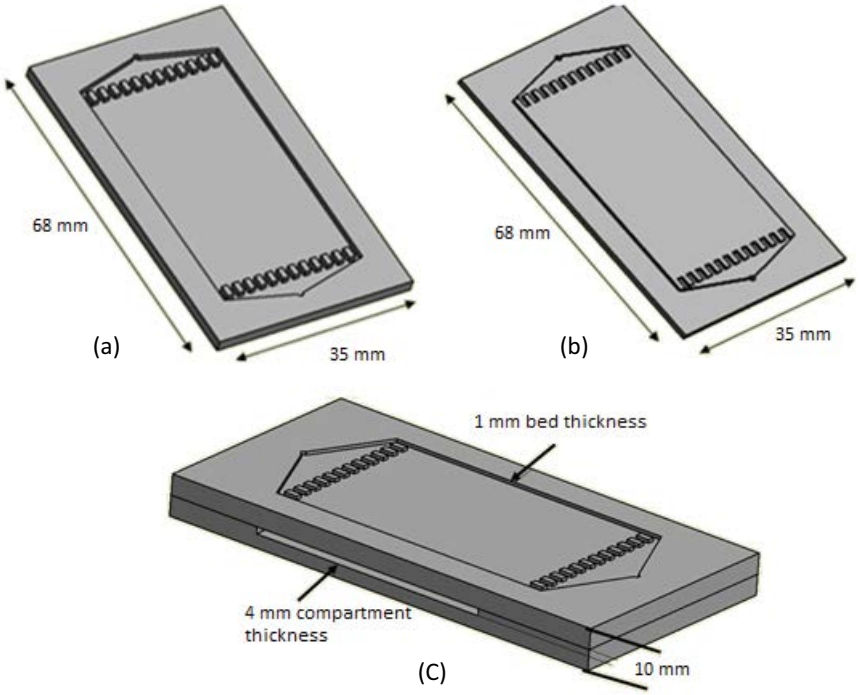

Fig. 1. Miniaturized flow cell (a) top view base part, (b) top view cover part, and (c) side view base part.

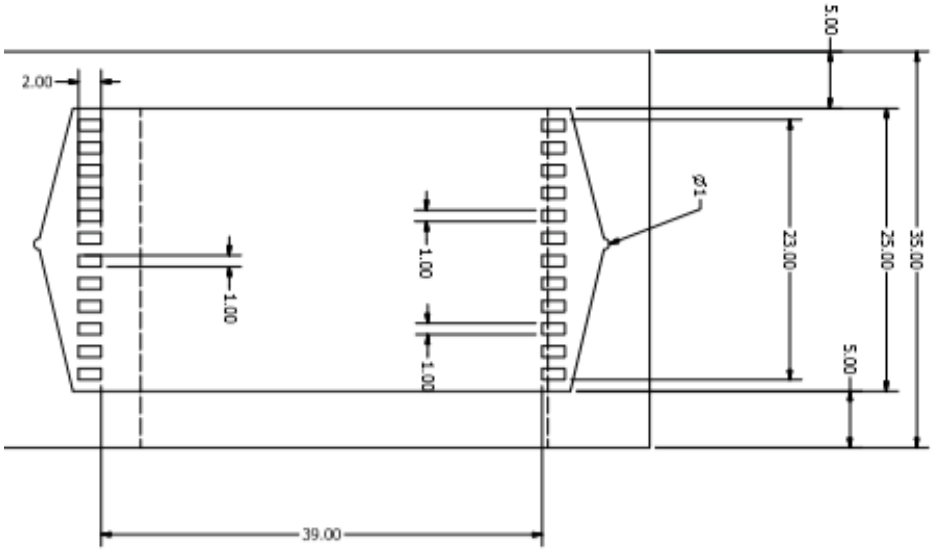

Fig. 2. Dimensions of the miniaturized flow cell active area (top view), in mm.

(Qualtech Products Industry, UK). Following this, the NPs with the adsorbed heavy metal ions were separated from the mixture and the residual heavy metals in the solution were determined by atomic adsorption spectroscopy (AAS). The adsorption efficiency (%*A*) was calculated as follows:

$$\%A = \frac{C_i - C_t}{C_i} \times 100 \quad (1)$$

where C_i (mg/L) is the initial concentration of the metal ions, and C_t (mg/L) is the concentration of the metal ions at a given time.

The effect of solution pH on the adsorption efficiency of heavy metal ions was investigated at different pH values in the range of 4–8. The pH of the 4 mg metal nitrate solution was adjusted using 0.05 M NaOH or 0.1 M HCl stock solutions. pH measurements were performed with a Metrohm 691 pH meter. The solution containing the NPs

Table 1
Dimensions of the fabricated miniaturized flow cell

Part	Dimensions (mm)				
	Width	Length	Depth	Height	Thickness
Cover	35	68	–	0.5	11.5
Base	35	68	1	–	10
Bed	23	39	0.5	–	
Magnet compartment	30	35			4

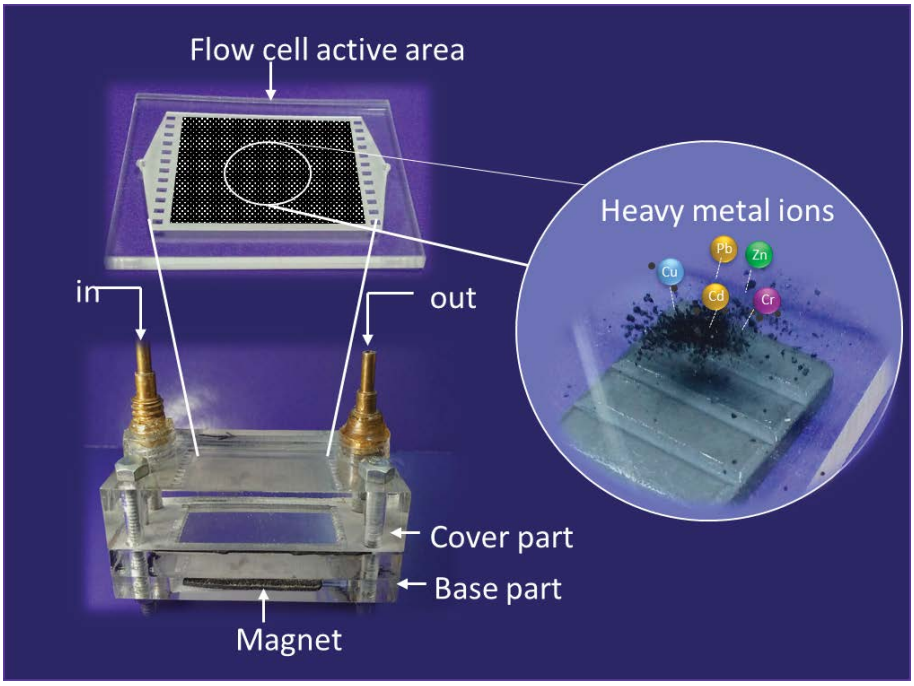

Fig. 3. Complete miniaturized flow cell.

was stirred for 10 min after which the adsorption efficiency was measured.

2.5.2. Continuous experiments

Continuous flow experiments were conducted in the designed flow cell based on the optimized pH obtained from the batch experiments. To study the effect of flow rate, 4 mg/L single heavy metal solution was treated in the flow cell for 15 min and different flow rates (19, 16, and 13 μL/s respectively) were adjusted by means of a peristaltic pump (Cole-Parmer Variable Flow pump, UK, Model: EW-73160–40). The treated solutions were then analyzed using AAS.

In order to evaluate the applicability of the proposed NPs for multiple removals of heavy metal ions and for real wastewater samples application, a synthetic heavy metal mixture and a real sample of wastewater were treated in the flow cell for 15 min at 13 μL/s.

The performance of the miniaturized flow cell was evaluated by measuring its capacity for continuous treatment as well as its capability for efficient regeneration. The former was performed by passing a Pb(II) and Cd(II) solution over the NPs in the flow cell for 2 h, while the latter was carried out by flushing the system with different concentrations of hydrochloric acid solutions.

2.5.3. Adsorption isotherms and kinetics

In order to examine the adsorption behavior of the magnetic-nanoparticles, 4 mg/L of each heavy metal solution was mixed with 10 mg of NPs and allowed to agitate for different periods of time, varying from 10 to 60 min at a constant speed of 500 rpm. Accordingly, the concentration of the heavy metal ion was recorded at different time intervals. The adsorption capacity which is defined as the amount of heavy metal ions adsorbed q (mg/g) was then calculated as:

$$q = \frac{\left(C_i - C_t\right) \times V}{m} \tag{2}$$

where q (mg/g) is the amount of metal ion adsorbed per unit amount of adsorbents, V (L) is the volume of adsorbates,

m (g) is the mass of adsorbent. All experiments were conducted in batch mode at room temperature and under optimum pH.

3. Results and discussion

3.1. Characterization

3.1.1. XRD analysis

The XRD pattern of the as-synthesized pure and Co-doped $MnFe_2O_4$ NPs prepared by microwave-assisted combustion method is shown in Fig. 4. Mainly, two phases are obtained, namely the major spinel phase $MnFe_2O_4$ with cubic structure and minor hematite phase α-Fe_2O_3. The main diffraction peaks at 2θ values about 29.65, 35.71, 37.02, 42.51, 53.05, 56.54, 62.05,70.52, 74.02 and 79.03 are ascribed to (220), (311), (222), (400), (422), (511), (440), (620), (533) and (444) planes, respectively which are characteristics of the cubic structure [1]. This is in agreement with JCPDS card No. 74–2403 and 22–1086 for $MnFe_2O_4$ and $CoFe_2O_4$, respectively. However, the small major peak around 2θ = 20.00 belongs to α-Fe_2O_3 phase, as a result of the partial oxidation of $MnFe_2O_4$ and Co-doped $MnFe_2O_4$ [32]. The peaks sharpness indicates the higher crystallinity of the as-prepared powders.

The intense main diffraction peaks (311) is used to calculate the crystallite size (L) following the Scherrer formula:

$$L = \frac{0.89\lambda}{\beta\cos\theta} \quad (3)$$

where λ is the wavelength, β is full width half maximum, and θ represents the diffraction angle. The estimated average crystallite size is found to be 60, 42, 39, 48 nm, respectively with increasing Co concentration. It is observed that the crystallite size decreases with the incorporation of Co^{2+} ions (x = 0.02, 0.06) within $MnFe_2O_4$ host lattice, which may be due to the lower concentration of the dopant that retards grain growth during the synthesis process. With a further increase in Co^{2+} concentration (x = 0.10), the crystallite size increases up to 48 but remains lower than that of pure $MnFe_2O_4$. In this case, it seems that higher Co^{2+} ions concentration favors grain growth at nucleation centers. The calculated average crystallite sizes good in agreement with the values obtained by the Rietveld analysis.

3.1.2. Rietveld analysis

The refinements of XRD patterns are carried out using the Rietveld method, as shown in Fig. 5. Rietveld refinement analysis is defined by the goodness of fit using the reliability factors $S = R_{wp}/R_e$, where R_{wp} and R_e are the R-weighted and the R-expected patterns, respectively. The calculated value of the lattice parameter and microstrain are listed in Table 2. The lattice parameter value of pure $MnFe_2O_4$ is 8.477 Å, which decreases with increasing the concentration of Co^{2+} ions, thereby obeyed Vegard's law [33]. The slight decrease in the lattice parameter can be attributed to the difference in ionic radii, so the larger ions of Mn^{2+} (r^{2+}_{Mn} = 0.83 Å) are replaced by smaller ions of Co^{2+} (r^{2+}_{Co} = 0.78 Å), resulting in lattice contraction [34]. Zhuang et al. [35] reported that the lattice parameter of $MnFe_2O_4$ is found to decrease with increasing the concentration of Zn^{2+} .

3.1.3. SEM observations

SEM images of pure and Co-doped $MnFe_2O_4$ powders as shown in Fig. 6, reveal that all the compositions exhibit spherical-like nanoparticles with a high tendency to agglomeration. All the images show variation in the particle size

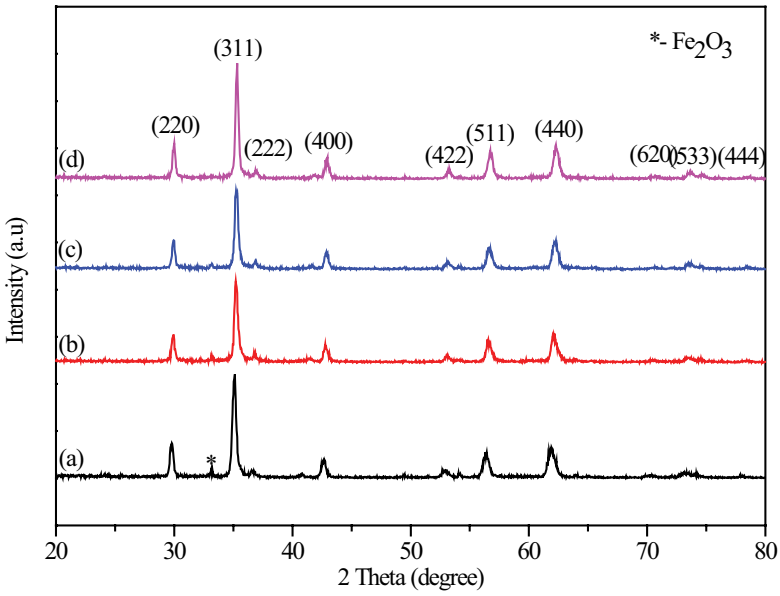

Fig. 4. X-ray diffraction patterns of as-prepared Co-doped $MnFe_2O_4$ nanopowders (a) $MnFe_2O_4$, (b) $Mn_{0.98}Co_{0.02}Fe_2O_4$, (c) $Mn_{0.94}Co_{0.06}Fe_2O_4$ and (d) $Mn_{0.90}Co0.10Fe_2O_4$.

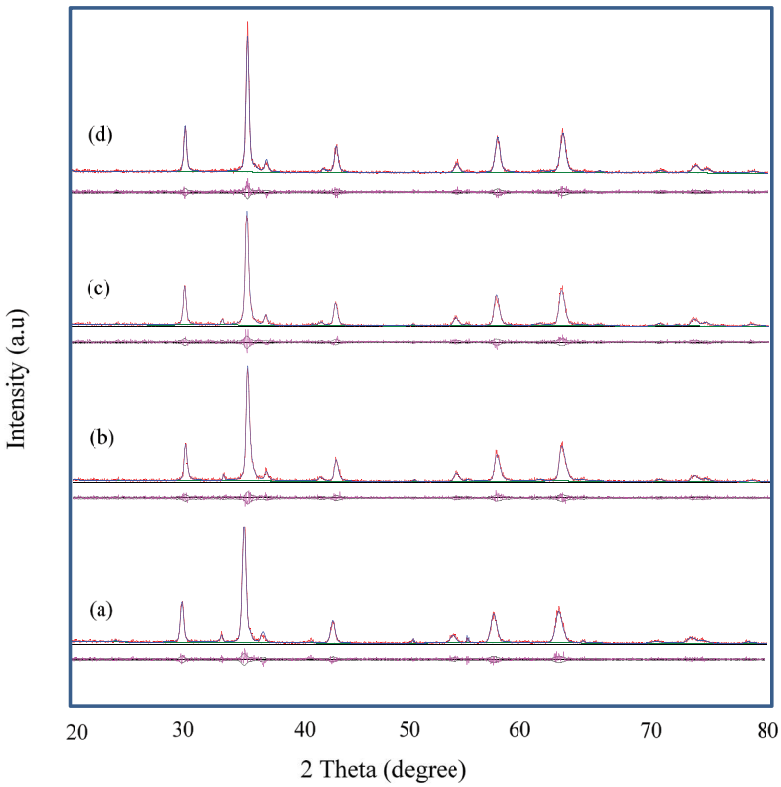

Fig. 5. Refined XRD patterns of as-prepared Co-doped $MnFe_2O_4$ nanopowders (a) $MnFe_2O_4$, (b) $Mn_{0.98}Co_{0.02}Fe_2O_4$, (c) $Mn_{0.94}Co_{0.0}6Fe_2O_4$ and (d) $Mn_{0.90}Co_{0.10}Fe_2O_4$. Solid red line represents the measured pattern, solid blue line represents the calculated pattern, and the difference between the observed and calculated is shown in the pink line.

Table 2
Results of Rietveld analysis of as-prepared Co-doped $MnFe_2O_4$ nanopowders

Samples	Crystallite size (nm)	Microstrain (%)	Lattice parameter (Å)	Goodness of fit "*S*"
$MnFe_2O_4$	60	0.412	8.477	1.14
$Mn_{0.98}Co_{0.02}Fe_2O_4$	42	0.411	8.461	1.07
$Mn_{0.94}Co_{0.06}Fe_2O_4$	39	0.362	8.449	1.09
$Mn_{0.90}Co_{0.10}Fe_2O_4$	48	0.375	8.429	1.13

vividly and distinct from each other. The surface morphology of the particles indicates that they are well crystallized and possess an average grain size of less than 100 nm, with non-uniform size distribution. The formation of agglomerates can be seen with visible grain boundaries. When Co^{2+} ions are incorporated within $MnFe_2O_4$, the particle size decreases since the smaller ionic radius of Co^{2+} ions replace a larger ionic radius of Mn^{2+} ions. The crystallite size values obtained from XRD (Scherrer and Rietveld refinements) analysis are fairly consistent with the particle size obtained from SEM observations.

3.1.4. Magnetic properties

The magnetic properties are found to vary depending upon the cations distribution between the octahedral and tetrahedral sites of the spinel cubic structure, as well as the chemical composition. Also, depending on the occupancy of cations at octahedral and tetrahedral sites, the magnetic behavior may change accordingly, namely paramagnetic, diamagnetic, ferromagnetic, and ferrimagnetic. Most importantly, the chemical composition and cations distribution in addition to particle size (domain size) play an important role in determining the magnetic properties.

The magnetization-field (M-H) curves of pure and Co-doped $MnFe_2O_4$ nanoparticles recorded at room temperature and with an applied field range of –10/+10 kOe are shown in Fig. 7. It is clear from the shape of the hysteresis loop the existence of ordered domains and that all studied compositions exhibit a ferromagnetic order. The values of saturation magnetization (M_s), remanent magnetization (M_r), and coercivity (H_c) determined from M-H curves are listed in Table 3. Pure $MnFe_2O_4$ NPs possess lower saturation magnetization (57.17 emu/g) than after co-doping. The obtained M_s value (57.17 emu/g) is slightly higher than that of $MnFe_2O_4$ NPs prepared by the high-temperature thermal

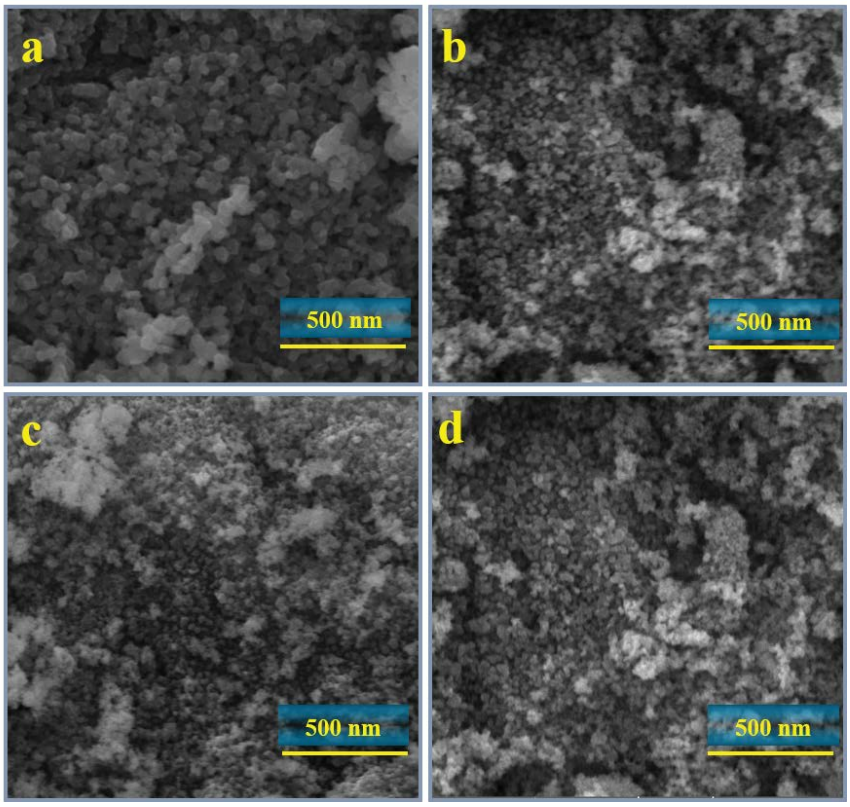

Fig. 6. SEM images of as-prepared Co-doped $MnFe_2O_4$ nanopowders.

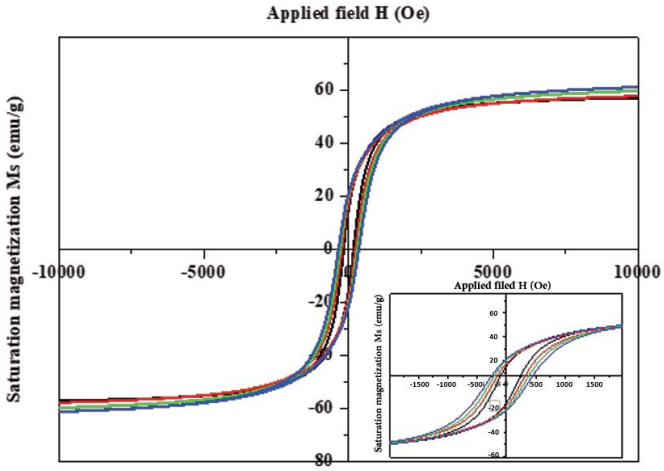

Fig. 7. M-H curves recorded at room temperature for as-prepared Co-doped $MnFe_2O_4$ nanopowders.

decomposition method (54.2 emu/g) [36] but much lower than that of $MnFe_2O_4$ NPs prepared by the hydrothermal route (72.45 emu/g) [37]. The difference in the observed values can be associated with extrinsic factors such as the preparation method, crystallinity, particle size and shape, as well as intrinsic parameters such as cations distribution among tetrahedral/octahedral sites, and local magnetic interactions.

Moreover, it is observed that the value of saturation magnetization increases with an increase in the concentration of Co^{2+} dopant. This is not expected, considering the lower magnetic moment of Co^{2+} (4.3–5.0 μ_B) replacing to Mn^{2+} (5.65–6.10 μ_B).

Moreover, it has been reported that Fe^{3+} ions with a higher magnetic moment (5.7–6.0 μ_B) can be replaced by Co^{2+} ions with a lower magnetic moment in the octahedral sublattice in $CoFe_{2-x}Zn_xO_4$ system, hence resulting in lower saturation magnetization [38]. However, according to spectroscopic study in the literature, Co^{2+} ions more preferably occupy octahedral sites than Mn^{2+} and Fe^{3+} ions

Table 3
Magnetic properties as determined from M-H curves of as-prepared Co-doped $MnFe_2O_4$ nanopowders

Samples	H_c (O_e)	M_r (emu/g)	M_s (emu/g)
$MnFe_2O_4$	118.2	15.60	57.17
$Mn_{0.98}Co_{0.02}Fe_2O_4$	235.6	17.98	57.78
$Mn_{0.94}Co_{0.06}Fe_2O_4$	290.7	20.54	59.77
$Mn_{0.90}Co_{0.10}Fe_2O_4$	349.3	21.62	61.17

in $CoFe_2O4$, $CoCr_{0.2}Fe_{1.8}O_4$ and $CoMn_{0.2}Fe_{1.8}O_4$ systems [39]. This means a possible occurrence of complex redistribution of metal ions among tetrahedral and octahedral sites within a $MnFe_2O_4$ crystal structure, but the most likely possibility resulting in the slight increase of M_s value from 57.17 up to 61.17 emu/g (7%) would be simultaneous occupancy of Mn^{2+} into Fe^{3+} and vice versa, as both ions possess slight differences in magnetic moments.

Similarly, the value of coercivity increases with increasing the concentration of the dopant. This might be due to the increase in the magnetic crystalline anisotropy which is correlated with a spin-orbital contribution [36]. Finally, it is concluded that, the values of saturation magnetization, coercivity and remanent magnetization increase with the increase in the concentration of the dopant.

3.2. Adsorption experiments

3.2.1. Effect of pH on the adsorption efficiency

The effect of pH on the heavy metal adsorption efficiency is illustrated in Fig. 8. It is apparent that the adsorption efficiency is highly affected by the solution pH. Overall, better removal is observed in neutral to alkaline media depending on the type of heavy metal ion, with the exception for Cd(II) and Zn(II) ions. One of the reasons for the low adsorption efficiency in the acidic media could be related to the repulsive forces between the positively charged surface NPs and the positive metal ions [40]. However, with the increase in pH, the surface charge of the active sites on the NPs becomes more negative thereby enhancing the attraction of the positively charged metal ions [41]. However, with the increase in pH, the surface charge of the active sites on the NPs become more negative thereby enhancing the attraction of the positively charged metal ions.

The adsorption efficiency of Cd(II) seems to be non-dependant on pH as almost 100% efficiency is observed at the investigated pH range [42], while that of Zn(II) shows 20% increase in the adsorption efficiency under alkaline conditions. Generally, the adsorption of Cd(II) is low in acidic media yet is raised with an increase of solution pH [43]; however, for the investigated range (pH 4–8) the adsorption efficiency seems not to vary with pH. In recent work by Wu et. al [44], a similar trend was reported for the adsorption of Cd(II) with in the investigated range. Huang and Keller [27] illustrated the steady adsorption of Cd(II) for pH range between 4 to 7.

For Pb(II) and Cu(II) ions, the adsorption efficiency continues to improve with the increase in solution pH. Similar observations were reported by Liu et al. [25]. However, for other metals like Co(II) and Cr(III), the maximum degradation is observed under neutral conditions after which it starts to decrease. Almost 80% reduction in the adsorption efficiency is observed for Cr(III) when the pH increased from 7 to 8. Depending on the pH value, the dominant form of Co(II) can vary between Co^{2+}, $Co(OH)^+$, $Co(OH)_2$, and $Co(OH)^{3-}$. At pH values less than 8, the predominant species are Co^{2+} and $Co(OH)^+$ however, in alkaline conditions, as a result of hydrolysis, the other forms of Co(II) ions will compete in the solution [45,46] Thus, the slight reduction in the adsorption of Co(II) at pH 8 can be due to the electrostatic repulsion among the negatively charged $Co(OH)^{3-}$ and the nanoparticles or the precipitation of $Co(OH)_2$ [47]. Similarly, in alkaline conditions, some part of Cr(III) ions can hydrolyze to $Cr_3(OH)_4^{5+}$, $CrOH^{2+}$, and $Cr(OH)_2^+$ where these ions become more predominant in the solution and less attractive to the surface of the nanoparticles [48,49]. Choudhury et al. [50] also had similar observations, where the maximum adsorption of Cr(III) was obtained at a pH of 7 after which the adoption started to decrease with the increase in the pH. Since the increase

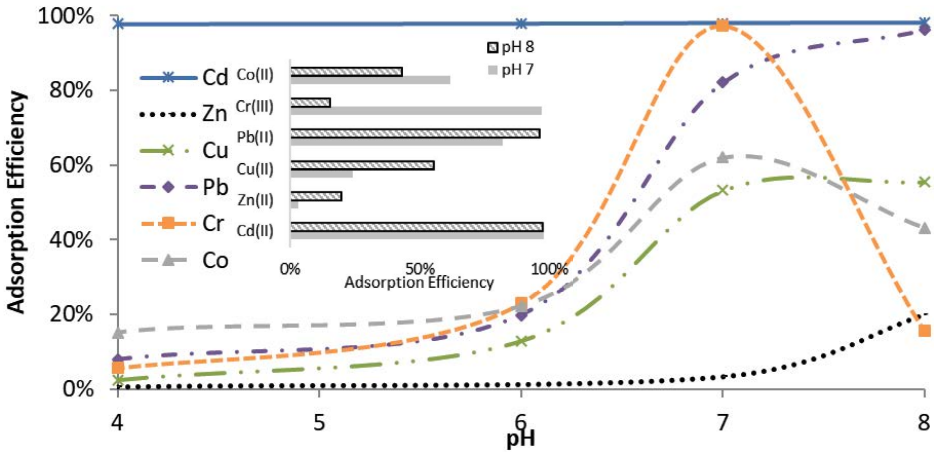

Fig. 8. Effect of pH on the heavy metal adsorption efficiency. Conditions: 4 ppm initial concentration; 10 mg nanoparticle dosage; 10 min adsorption time. Inset: adsorption efficiency at pH 7 and 8.

in adsorption efficiency for Pb(II) and Cu(II)is not considerably higher with the increase in pH, a pH value of 7 has been selected as the optimum value for future experiments.

3.2.2. Effect of contact time on the adsorption efficiency

The time dependence of adsorption is an important factor for the identification of the rapidness of adsorption processes, as well as the optimum time necessary for maximum removal of the target heavy metal ion. As illustrated in Fig. 9, for most heavy metals, a rapid increase in the adsorption efficiency is observed at the initial stages, followed by a gradual increase leading to an equilibrium plateau. The rapid adsorption efficiency is perhaps due to external surface adsorption. Since nearly all of the adsorption sites of magnetic NPs exist on the exterior of the adsorbent compared to the porous adsorbent, it is easy for the adsorbate to access the active sites, leading to a rapid approach to equilibrium. With longer contact time, as the most active sites of the adsorbent become occupied by the adsorbate, the adsorption capacity declines gradually until a plateau is reached indicating the saturation of the active sites [27]. Similar rapid adsorption rates have been reported in the literature [51]. Table 4 shows the equilibrium adsorption for the investigated heavy metal ions. Rapid equilibrium adsorption, within 10 min is achieved for Cd(II), Cr(III) and Pb(II). At equilibrium, the amount of adsorbed Cd(II), Cr(III) and Pb(II) is found to be 98, 94 and 82%, respectively, whereas, slower equilibrium is achieved for Co(II) and Cu(II), within 40 min, but with high removal efficiencies of 95.0 and 96% respectively. On the other hand, Zn(II) reaches only 20% absorption efficiency within the initial 10 min and took 50 min to reach equilibrium at 90.9%. Huang and Keller [27] obtained similar results but the equilibrium adsorption was achieved much longer, around 2 h. Similarly, Wang et al. [52] achieved an equilibrium for Pb(II) and Cu(II) within an even longer contact time of 3 h.

3.2.3. Effect of solution flow rate on the adsorption efficiency

Fig. 10 illustrates the effect of the solution flow rate on the heavy metal adsorption efficiency in the designed microfluidic system. It is clear that the adsorption efficiency is the highest for all the investigated heavy metal ions at the lowest flow rate, that is, at 13 μL/s. This could be attributed to the fact that since the flow rate is low, the residence time of the heavy metals in the microfluidic system increases, allowing better contact with NPs, which leads to high adsorption performance. The opposite is also true, that is, with increasing the flow rate, the diffusion rate of the solution increases and the adsorption slows down gradually, which can be explained by the lower contact time for heavy metal ions to interact with the active sites at the surface of NPs.

3.2.4. Flow cell adsorption efficiency for single and multiple heavy metal removal

In real waste samples, competitive ions are expected to coexist and may affect the adsorption of each other. For example, heavy transition metal ions such as Cu(II), Zn(II), and Pb(II) may compete with each other causing partial absorption or unequal adsorption onto NPs [53]. Therefore, the selectivity of the microfluidic system for single and multiple metals adsorption in synthetic and real solutions has been investigated at an optimum flow rate of 13 μL/min. The synthetic mixture solution contains some representative heavy metal ions based on the single metal experiments and the real sample solution. On the other hand, the real wastewater sample is directly taken from the Muharraq Wastewater Treatment Plant. The selectivity results for the single metal adsorption using the microfluidic system are shown in Table 5, while that of the synthetic mixture and real sample are illustrated in Fig. 11.

For the single heavy metal solutions, the adsorption order is found as follows:

Cr(III) > Cd(II) > Pb(II) > Co(II) > Cu(II) > Zn(II)

While in synthetic mixture, the adsorption order is found as follows:

Pb(II) > Cu(II) > Co(II) > Cd(II)

The results indicate that the nanoparticles have more affinity for Pb(II) than the other heavy metals in the solution. This adsorption order seems to very well agree with previous work published by Giraldo et al. [54] and Wang et al. [55]. It was suggested that the size of the hydrated ionic radii could highly affect its interaction with the negatively charged adsorption site. They proposed that as the size of the

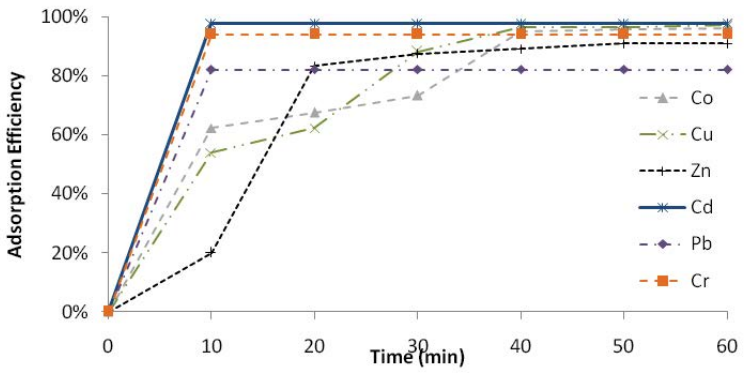

Fig. 9. Effect of contact time on the heavy metal adsorption efficiency. Conditions: optimum pH of 7, other conditions as described in Fig. 8.

ion's hydration increases, its distance from the adsorbing surface increases too thus, its adsorption becomes weaker [54].

The real wastewater contains only two of the heavy metals, namely Cd(II) and Cu(II), which are found to be completely adsorbed onto the magnetic nanoparticles. This Indicates that the synthesized nanoparticles are equally good for the removal of Cu(II) and Cd(II) mixed solution. However, in the presence of other competing ions, the adsorption selectivity of these nanoparticles seems to vary as discussed earlier.

3.2.5. Regeneration of NPs

Fig. 12 depicts the adsorption efficiency of NPs with respect to time. It can be noted that with increasing the contact time, the active sites available to NPs became

Table 4
Equilibrium time and maximum adsorption efficiency of different heavy metals

	Equilibrium time (min)	Adsorption efficiency (%)
Cd(II)	10	98
Cu(II)	40	96
Co(II)	40	95
Cr(III)	10	94
Zn(II)	50	91
Pb(II)	10	82

Table 5
Adsorption efficiency of the flow cell for single heavy metal ion solutions

Heavy metal	Adsorption efficiency (%)
Cr(III)	94
Cd (II)	87
Pb(II)	76
Co(II)	56
Cu(II)	46
Zn(II)	20

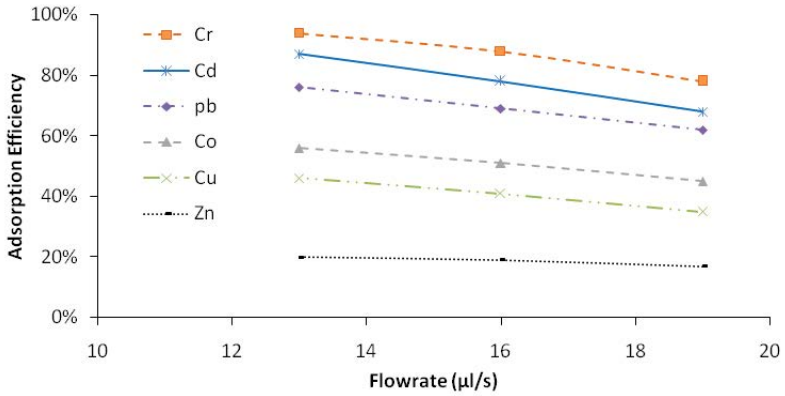

Fig. 10. Effect of solution flow rate in the flow cell on the heavy metal adsorption efficiency. Conditions: optimum pH of 7; 4 ppm initial concentration; 30 mg nanoparticle dosage; 15 min contact time.

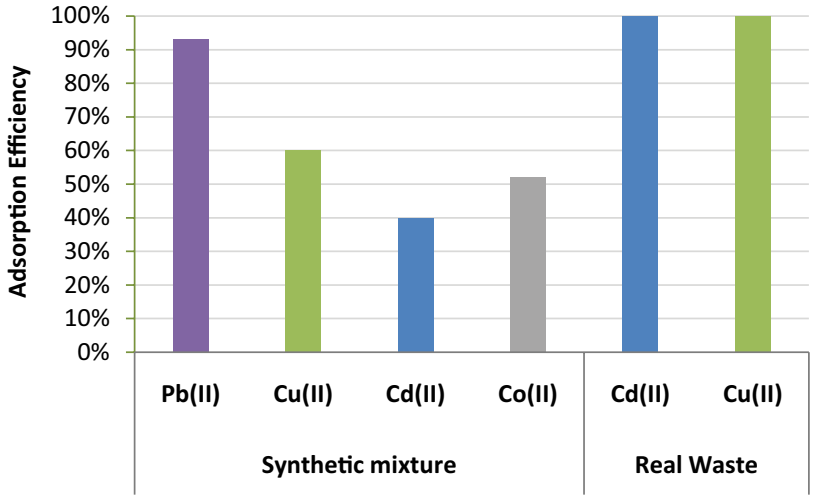

Fig. 11. The selectivity of the flow cell for multiple heavy metal adsorption. Conditions: as described in Fig. 10.

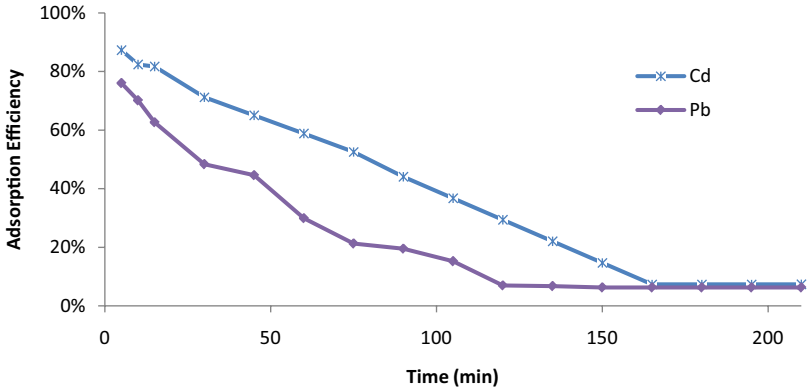

Fig. 12. Adsorption efficiency of NPs within the flow cell with respect to time. Conditions: as described in Fig. 10.

occupied by heavy metal ions thereby decreasing the adsorption rate. Thus, the reuse of the adsorbent through the regeneration of its adsorption properties is an economic necessity. Desorption of metal ions in acidic media appeared to be rapid and high [56]; at low pH, strong competition between H^+ ions and metal cations for adsorption sites causes displacement of cations into the acid solution. Therefore, various concentrations of HCl are used for the regeneration of magnetic NPs as shown in Fig. 13. The adsorption efficiency is found to be higher for the NPs regenerated using a high acid concentration in comparison to lower concentration. Approximately, 75% adsorption efficiency of Pb(II) is recovered after the regeneration of NPs using acid concentrations of 0.05 M and more, in comparison to 76% adsorption efficiency using fresh NPs. This indicates an efficient regeneration process.

3.3. Adsorption isotherms and kinetics

3.3.1. Adsorption isotherms

Adsorption isotherms describe how solutes interact with the sorbent and are defined as the relation between the amount of the adsorbate on the adsorbent at constant temperature and the concentrations of the adsorbate in the equilibrium solution. Adsorption isotherms are important for analyzing the adsorption capacity of the adsorbents. Various models were developed for describing the adsorption isotherms, of which the Langmuir and Freundlich models are the most extensively used [12,22]. The Langmuir model assumes monolayer uniform adsorption while the Freundlich isotherm model describes the non-ideal sorption behavior and assumes multilayer adsorption.

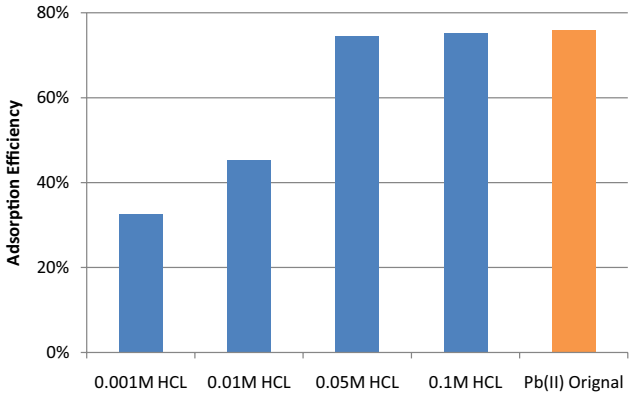

Fig. 13. Adsorption efficiency of the regenerated NPs for Pb(II) ions after treatment with different HCl concentrations in comparison to the freshly used NPs.

The Langmuir and Freundlich equation is expressed by the following equations, respectively [22]:

$$\frac{C_e}{q_e} = \frac{1}{Q_0 \times b} + \frac{C_e}{Q_0} \tag{4}$$

where C_e (mg/L) is the equilibrium concentration, q_e (mg/g) is the amount of adsorbate adsorbed per unit mass of adsorbate, Q_0 and b are the Langmuir constants related to the adsorption capacity and the rate of adsorption, respectively. If the adsorption system follows a Langmuir adsorption model, then a plot of C_e/q_e vs. C_e would produce a straight line from which the constants could be evaluated.

Another important parameter, R_L, called the separation factor, is determined from the following relation [22]:

$$R_L = \frac{1}{1 + \left(b \times C_0\right)} \tag{5}$$

In general,

If $0 < R_L < 1$, then the adsorption characteristic is favourable;

If $R_L = 0$, then the adsorption characteristic is irreversible;

If $R_L = 1$, then the adsorption characteristic is linear;

If $R_L > 1$, then the adsorption characteristic is unfavourable;

The linear form of the Freundlich equation is [36]:

$$\ln q_e = \ln K_F + \frac{1}{n} \ln C_e \tag{6}$$

where K_F and n are Freundlich constants, where K_F (mg/g) is the adsorption capacity of the adsorbent and n giving an indication of how favorable the adsorption process is [36].

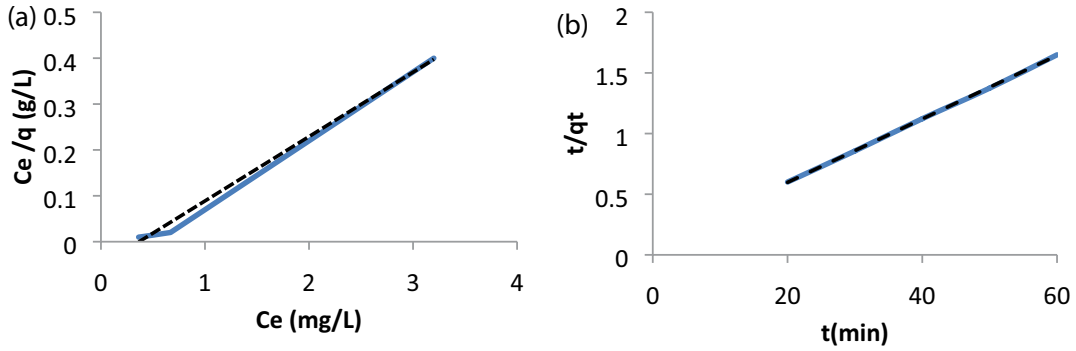

Fig. 14. (a) Linearized Langmuir isotherms for the adsorption of Zn(II) and (b) pseudo-second-order model for the absorption of Zn(II) Conditions: as described in Fig. 8.

If the adsorption system follows the Freundlich model, then a plot of $\ln q_e$ vs. $\ln C_e$ would give a straight line from which the constants K_F and n could be evaluated.

In this work, the Langmuir and Freundlich adsorption isotherms are used to describe the distribution of the adsorbate species among the liquid and the adsorbent. These isotherms relate heavy metal uptake per unit mass of adsorbent to the adsorbate concentration in the fluid. Cobalt, copper and zinc have been selected as representative heavy metal samples for this purpose.

The linear fitting curve of the Langmuir model for the adsorption of Zn(II) ions on magnetic NPs is shown in Fig. 14a, while the regression coefficients (R^2) and the model constants for the three representative ions are summarized in Table 6. The straight-line plot and the R^2 values indicate that the adsorption of the representative ions on NPs follows the Langmuir isotherm, suggesting a monolayer sorption mechanism, where the adsorption takes place uniformly on the active sites of the magnetic NPs [25]. According to this model, once the active sites are occupied by the heavy metal ions, there will be no more adsorption behavior on these sites. Moreover, the calculated R_L values, for the representative metal ions, as shown in Table 6, are less than 1 and greater than zero, indicating favorable adsorption. On the other hand, although the Freundlich isotherm model gave R^2 greater than 0.9, the slopes were negative suggesting the invalidity of the model for the given sample.

3.3.2. Adsorption kinetics models

The determination of kinetics is vital for the design of adsorption systems and the reaction rate-controlling step as the chemical reaction occurs [22]. Adsorption kinetics is important for designing and modeling the adsorption process. It describes the relation between the amount of substance adsorbate adsorbed on the adsorbent with respect to the contact time (t). The frequently used adsorption kinetics include the pseudo-first-order and pseudo-second-order kinetic described by the following equations respectively [22]:

$$\ln\left(q_e - q_t\right) = \ln q_e - k_1 t \tag{7}$$

where q_t is the amount adsorbate adsorbed on the adsorbent at time t, and k_1 is the rate constant of the pseudo-first-order model for the adsorption (min^{-1}):

$$\frac{t}{q_t} = \frac{1}{k_2 \times q_e^2} + \frac{t}{q_e} \tag{8}$$

where k_2 is the rate constant of the pseudo-second-order model for adsorption (g/mg min).

Both models are used to evaluate the kinetics of the heavy metal removal process. The obtained results reveal a better fit of the experimental data on the pseudo-second-order kinetic models as indicated in Fig. 14b and the R^2 values in Table 6. This suggests that the adsorption processes are dominated by the chemical process (chemisorption). Similar observations were reported in the literature for copper ions [25,31].

4. Conclusion

Magnetic ferrite nanoparticles with a promising adsorption performance were successfully synthesized and

Table 6
Adsorption isotherms and kinetics parameters

Metals	Langmuir isotherm			Pseudo-second-order kinetics		
	R^2	Q_0 (mg/g)	R_L	R^2	Slope (g/mg)	Intercept (min g/mg)
Zn(II)	0.994	7.140	0.034	0.9998	0.0262	0.0745
Cu(II)	0.989	21.74	0.011	0.9583	0.0233	0.1564
Co(II)	0.992	25.00	0.101	0.9626	0.0243	0.1402

evaluated for the removal of different heavy metal ions in synthetic and real solutions. A dedicated designed flow cell was fabricated and utilized as a continuous adsorption system. Nanoparticles were detained in position inside the flow cell by the application of a magnetic field. Favorable pH value of 7 and absorption efficiencies of higher than 90% were achieved with almost all the investigated metal ions.

The miniaturized flow cell proved its applicability for the continued removal of heavy metal ions in single and multiple solutions. The adsorption of selected ions onto magnetic ferrite nanoparticles seemed to follow pseudo-second-order kinetics and was well described by the Langmuir isotherm model. The flow cell containing nanoparticles demonstrated its compatibility for real wastewater treatment.

References

[1] A.J. Bora, R.K. Dutta, Removal of metals (Pb, Cd, Cu, Cr, Ni, and Co) from drinking water by oxidation-coagulation-absorption at optimized pH, J. Water Process Eng., 31 (2019) 100839.

[2] F. Fu, Q. Wang, Removal of heavy metal ions from wastewaters: a review, J. Environ. Manage., 92 (2011) 407–418.

[3] C.F. Carolin, P.S. Kumar, A. Saravanan, G.J. Joshiba, M. Naushad, Efficient techniques for the removal of toxic heavy metals from aquatic environment: a review, J. Environ. Chem. Eng., 5 (2017) 2782–2799.

[4] A. Selimović, H. Junuzović, S. Begić, R. Cvrk, Efficiency of precipitation and removal of Pb(II) and Zn(II) ions from their monocomponent and two-component aqueous solutions using Na_2CO_3, Lect. Notes Networks Syst., 76 (2020) 569–575.

[5] X. Li, Q. Zhang, B. Yang, Co-precipitation with $CaCO_3$ to remove heavy metals and significantly reduce the moisture content of filter residue, Chemosphere, 239 (2020) 124660.

[6] E. Jashni, S.M. Hosseini, Promoting the electrochemical and separation properties of heterogeneous cation exchange membrane by embedding 8-hydroxyquinoline ligand: chromium ions removal, Sep. Purif. Technol., 234 (2020) 116118.

[7] Q. Chen, Z. Tang, H. Li, M. Wu, Q. Zhao, B. Pan, An electron-scale comparative study on the adsorption of six divalent heavy metal cations on $MnFe_2O_4$@CAC hybrid: experimental and DFT investigations, Chem. Eng. J., 381 (2020) 122656.

[8] F. Wu, T. Zhao, Y. Yao, T. Jiang, B. Wang, M. Wang, Recycling supercapacitor activated carbons for adsorption of silver(I) and chromium(VI) ions from aqueous solutions, Chemosphere, 238 (2020) 124638.

[9] X. Liu, B. Jiang, X. Yin, H. Ma, B.S. Hsiao, Highly permeable nanofibrous composite microfiltration membranes for removal of nanoparticles and heavy metal ions, Sep. Purif. Technol., 233 (2020) 115976.

[10] X. Su, A. Kushima, C. Halliday, J. Zhou, J. Li, T.A. Hatton, Electrochemically-mediated selective capture of heavy metal chromium and arsenic oxyanions from water, Nat. Commun., 9 (2018) 4701.

[11] L.A. Malik, A. Bashir, A. Qureashi, A.H. Pandith, Detection and removal of heavy metal ions: a review, Environ. Chem. Lett., 17 (2019) 1495–1521.

[12] A.E. Burakov, E.V. Galunin, I.V. Burakova, A.E. Kucherova, S. Agarwal, A.G. Tkachev, V.K. Gupta, Adsorption of heavy metals on conventional and nanostructured materials for wastewater treatment purposes: a review, Ecotoxicol. Environ. Saf., 148 (2018) 702–712.

[13] M. Naushad, Z.A. Alothman, Separation of toxic Pb^{2+} metal from aqueous solution using strongly acidic cation-exchange resin: analytical applications for the removal of metal ions from pharmaceutical formulation, Desal. Water Treat., 53 (2015) 2158–2166.

[14] H. Esmaeili, R. Foroutan, Investigation into ion exchange and adsorption methods for removing heavy metals from aqueous solutions, Int. J. Biol. Pharm. Allied Sci., 4 (2015) 620–629.

[15] J. Beltrán Heredia, J. Sánchez Martín, Removing heavy metals from polluted surface water with a tannin-based flocculant agent, J. Hazard. Mater., 165 (2009) 1215–1218.

[16] D.S. Patil, S.M. Chavan, J.U.K. Oubagaranadin, A review of technologies for manganese removal from wastewaters, J. Environ. Chem. Eng., 4 (2016) 468–487.

[17] A.A.H. Faisal, S.F.A. Al-Wakel, H.A. Assi, L.A. Naji, M. Naushad, Waterworks sludge-filter sand permeable reactive barrier for removal of toxic lead ions from contaminated groundwater, J. Water Process Eng., 33 (2020) 101112.

[18] S. Wadhawan, A. Jain, J. Nayyar, S.K. Mehta, Role of nanomaterials as adsorbents in heavy metal ion removal from waste water: a review, J. Water Process Eng., 33 (2020) 101038.

[19] N. Gupta, P. Pant, C. Gupta, P. Goel, A. Jain, S. Anand, A. Pundir, Engineered magnetic nanoparticles as efficient sorbents for wastewater treatment: a review, Mater. Res. Innovations, 22 (2018) 434–450.

[20] A. Şen, H. Pereira, M.A. Olivella, I. Villaescusa, Heavy metals removal in aqueous environments using bark as a biosorbent, Int. J. Environ. Sci. Technol., 12 (2015) 391–404.

[21] M. Shafiq, A.A. Alazba, M.T. Amin, Removal of heavy metals from wastewater using date palm as a biosorbent: a comparative review, Sains Malaysiana, 47 (2018) 35–49.

[22] G.K. Sarma, S. Sen Gupta, K.G. Bhattacharyya, Nanomaterials as versatile adsorbents for heavy metal ions in water: a review, Environ. Sci. Pollut. Res., 26 (2019) 6245–6278.

[23] Y. Wu, H. Pang, Y. Liu, X. Wang, S. Yu, D. Fu, J. Chen, X. Wang, Environmental remediation of heavy metal ions by novel-nanomaterials: a review, Environ. Pollut., 246 (2019) 608–620.

[24] S. Tamjidi, H. Esmaeili, B. Kamyab Moghadas, Application of magnetic adsorbents for removal of heavy metals from wastewater: a review study, Mater. Res. Express, 6 (2019) 102004.

[25] F. Liu, K. Zhou, Q. Chen, A. Wang, W. Chen, Application of magnetic ferrite nanoparticles for removal of Cu(II) from copper-ammonia wastewater, J. Alloys Compd., 773 (2019) 140–149.

[26] N.A. Yazid, Y.C. Joon, Co-precipitation synthesis of magnetic nanoparticles for efficient removal of heavy metal from synthetic wastewater, AIP Conf. Proc., 2124 (2019) 1–10.

[27] Y. Huang, A.A. Keller, EDTA functionalized magnetic nanoparticle sorbents for cadmium and lead contaminated water treatment, Water Res., 80 (2015) 159–168.

[28] K. Kombaiah, J.J. Vijaya, L.J. Kennedy, M. Bououdina, R.J. Ramalingam, H.A. Al-Lohedan, Okra extract-assisted green synthesis of $CoFe_2O_4$ nanoparticles and their optical, magnetic, and antimicrobial properties, Mater. Chem. Phys., 204 (2018) 410–419.

[29] Y. Zhang, T. Yan, L. Yan, X. Guo, L. Cui, Q. Wei, B. Du, Preparation of novel cobalt ferrite/chitosan grafted with graphene composite as effective adsorbents for mercury ions, J. Mol. Liq., 198 (2014) 381–387.

[30] R. Bhateria, R. Singh, A review on nanotechnological application of magnetic iron oxides for heavy metal removal, J. Water Process Eng., 31 (2019) 100845.

[31] F. Almomani, R. Bhosale, M. Khraisheh, A. Kumar, T. Almomani, Heavy metal ions removal from industrial wastewater using magnetic nanoparticles (MNP), Appl. Surf. Sci., 506 (2020) 144924.

[32] H. Waqas, A.H. Qureshi, K. Subhan, M. Shahzad, Nanograin Mn-Zn ferrite smart cores to miniaturize electronic devices, Ceram. Int., 38 (2012) 1235–1240.

[33] M.A. Gabal, S.S. Ata-Allah, Effect of diamagnetic substitution on the structural, electrical and magnetic properties of $CoFe_2O_4$, Mater. Chem. Phys., 85 (2004) 104–112.

[34] L.B. Tahar, H. Basti, F. Herbst, L.S. Smiri, J.P. Quisefit, N. Yaacoub, J.M. Greneche, S. Ammar, $Co_{1-x}Zn_xFe_2O_4$ ($0 \le x \le 1$) nanocrystalline solid solution prepared by the polyol method: characterization and magnetic properties, Mater. Res. Bull., 47 (2012) 2590–2598.

[35] L. Zhuang, W. Zhang, Y. Zhao, D. Li, W. Wu, H. Shen, Temperature sensitive ferrofluid composed of $Mn_{1-x}Zn_xFe_2O_4$

nanoparticles prepared by a modified hydrothermal process, Powder Technol., 217 (2012) 46–49.
[36] H.N. Choi, K.S. Baek, S.W. Hyun, I.B. Shim, C.S. Kim, A study of Co substituted Mn-Ferrite, $Mn_{1-x}Co_xFe_2O_4$(x = 0.0,0.5,1.), IEEE Trans. Magn., 45 (2009) 2554–2556.
[37] L. Zhou, H.B. Wu, T. Zhua, X.W. Lou, Facile preparation of $ZnMn_2O_4$ hollow microspheres as high-capacity anodes for lithium-ion batteries, J. Mater. Chem., 22 (2011) 827–829.
[38] N. Somaiah, T.V. Jayaraman, P.A. Joy, D. Das, Magnetic and magnetoelastic properties of Zn-doped cobalt-ferrites—$CoFe_{2-x}Zn_xO_4$ (x = 0, 0.1, 0.2, and 0.3), J. Magn. Magn. Mater., 324 (2012) 2286–2291.
[39] A.M. Cojocariu, M. Soroceanu, L. Hrib, V. Nica, O.F. Caltun, Microstructure and magnetic properties of substituted (Cr, Mn) - cobalt ferrite nanoparticles, Mater. Chem. Phys., 135 (2012) 728–732.
[40] M. Dinari, R. Tabatabaeian, Ultra-fast and highly efficient removal of cadmium ions by magnetic layered double hydroxide/guargum bionanocomposites, Carbohydr. Polym., 192 (2018) 317–326.
[41] Y. Zhang, L. Yan, W. Xu, X. Guo, L. Cui, L. Gao, Q. Wei, B. Du, Adsorption of Pb(II) and Hg(II) from aqueous solution using magnetic $CoFe_2O_4$-reduced graphene oxide, J. Mol. Liq., 191 (2014) 177–182.
[42] D. Ouyang, Y. Zhuo, L. Hu, Q. Zeng, Y. Hu, Z. He, Research on the adsorption behavior of heavy metal ions by porous material prepared with silicate tailings, Minerals, 9 (2019) 1–16.
[43] Y. Feng, J.-L. Gong, G.-M. Zeng, Q.-Y. Niu, H.-Y. Zhang, C.-G. Niu, J.-H. Deng, M. Yan, Adsorption of Cd(II) and Zn(II) from aqueous solutions using magnetic hydroxyapatite nanoparticles as adsorbents, Chem. Eng. J., 162 (2010) 487–494.
[44] C. Wu, X. Wei, P. Liu, J. Tan, C. Liao, H. Wang, L. Yin, W. Zhou, H.-J. Cui, Influence of structural Al species on Cd(II) capture by iron muscovite nanoparticles, Chemosphere, 226 (2019) 907–914.
[45] Ş. Kubilay, R. Gürkan, A. Savran, T. Şahan, Removal of Cu(II), Zn(II) and Co(II) ions from aqueous solutions by adsorption onto natural bentonite, Adsorption, 13 (2007) 41–51.
[46] M. Xing, L. Xu, J. Wang, Mechanism of Co(II) adsorption by zero valent iron/graphene nanocomposite, J. Hazard. Mater., 301 (2016) 286–296.
[47] K. Chen, J. He, Y. Li, X. Cai, K. Zhang, T. Liu, Y. Hu, D. Lin, L. Kong, J. Liu, Removal of cadmium and lead ions from water by sulfonated magnetic nanoparticle adsorbents, J. Colloid Interface Sci., 494 (2017) 307–316.
[48] B. Eyvazi, A. Jamshidi-Zanjani, A. Khodadadi Darban, Synthesis of nano-magnetic $MnFe_2O_4$ to remove Cr(III) and Cr(VI) from aqueous solution: a comprehensive study, Environ. Pollut., (2019) 113685, (in Press).
[49] C. Bai, L. Wang, Z. Zhu, Adsorption of Cr(III) and Pb(II) by graphene oxide/alginate hydrogel membrane: characterization, adsorption kinetics, isotherm and thermodynamics studies, Int. J. Biol. Macromol., 147 (2020) 898–910.
[50] T.R. Choudhury, K.M. Pathan, M.N. Amin, M. Ali, S.B. Quraishi, A.I. Mustafa, Adsorption of Cr(III) from aqueous solution by groundnut shell, J. Environ. Sci. Water Res., 1 (2012) 144–150.
[51] H. Xu, H. Yuan, J. Yu, S. Lin, Study on the competitive adsorption and correlational mechanism for heavy metal ions using the carboxylated magnetic iron oxide nanoparticles (MNPs-COOH) as efficient adsorbents, Appl. Surf. Sci., 473 (2019) 960–966.
[52] N. Wang, D. Yang, X. Wang, S. Yu, H. Wang, T. Wen, G. Song, Z. Yu, X. Wang, Highly efficient Pb(II) and Cu(II) removal using hollow Fe_3O_4@PDA nanoparticles with excellent application capability and reusability, Inorg. Chem. Front., 5 (2018) 2174–2182.
[53] W. Fu, Z. Huang, One-pot synthesis of a two-dimensional porous Fe_3O_4/Poly($C_3N_3S_3$) network nanocomposite for the selective removal of Pb(II) and Hg(II) from synthetic wastewater, ACS Sustainable Chem. Eng., 6 (2018) 14785–14794.
[54] L. Giraldo, A. Erto, J.C. Moreno-Piraján, Magnetite nanoparticles for removal of heavy metals from aqueous solutions: synthesis and characterization, Adsorption, 19 (2013) 465–474.
[55] X.S. Wang, H.J. Lu, L. Zhu, F. Liu, J.J. Ren, Adsorption of lead(II) ions onto magnetite nanoparticles, Adsorpt. Sci. Technol., 28 (2010) 407–417.
[56] V. Srivastava, Y.C. Sharma, M. Sillanpää, Application of nano-magnesso ferrite (n-$MgFe_2O_4$) for the removal of Co^{2+} ions from synthetic wastewater: kinetic, equilibrium and thermodynamic studies, Appl. Surf. Sci., 338 (2015) 42–54.